Geosciences and Geological and Petroleum Engineering Faculty Research & Creative Works

Geosciences and Geological and Petroleum Engineering

01 Jan 2023

Analyzing Spatio-Temporal Mechanisms of Land Subsidence in the Parowan Valley, Utah, USA

Jiawei Li

Ryan G. Smith
Missouri University of Science and Technology, smithryang@mst.edu

Katherine R. Grote
Missouri University of Science and Technology, grotekr@mst.edu

Follow this and additional works at: https://scholarsmine.mst.edu/geosci_geo_peteng_facwork

🔴 Part of the Geological Engineering Commons, and the Petroleum Engineering Commons

Recommended Citation

PAPER

Analyzing spatio-temporal mechanisms of land subsidence in the Parowan Valley, Utah, USA

Jiawei Li[1] · Ryan Smith[1] · Katherine Grote[1]

Abstract

Parowan Valley, Utah (USA), is an agricultural region experiencing rapid subsidence due to extensive groundwater extraction from aquifers with a significant portion of fine-grained sediments. To analyze the subsidence spatio-temporally, time-series Interferometric Synthetic Aperture Radar (InSAR) of 155 Sentinel-1 C-band scenes were processed. These data showed approximately 30 cm of ground subsidence in Parowan Valley from 2014 to 2020. Because of the high temporal sampling rate of the Sentinel-1 satellite (12-day cycle), it is possible to determine the seasonal changes of ground deformation and relate this to groundwater extraction. To better understand the relationship between ground deformation and groundwater extraction in the Parowan Valley, temporal changes in hydraulic head data from US Geological Survey observation wells were monitored. Additionally, well logs were analyzed and used to construct a map that showed the percentage of fine-grained material in the subsurface. The investigation of hydraulic head and geology, together with InSAR-derived ground displacement data, indicates that the most subsidence occurs where there is a co-occurrence of high groundwater demand and a high percentage of fine-grained sediments, but recharge likely plays a role in mitigating subsidence in some areas. The subsidence developed in Parowan Valley shows a long-term trend as well as seasonal variation and appears to be influenced by both agricultural activity and annual precipitation.

Keywords Subsidence · InSAR · Groundwater · Agriculture · USA

Introduction

Overextraction of groundwater for irrigation has been recognized as a major driver of ground deformation and land subsidence in agricultural areas (Bouwer 1977; Khan et al. 2013; Faunt et al. 2016). The hazards of land subsidence have been examined in numerous studies. These hazards include the development of earth fissures (Conway 2016; Youssef et al. 2013), reduction of aquifer storage (Holzer and Galloway 2005), flooding (Anzidei et al. 2017), and damage to architectural structures, foundations, drainage canals, pipelines, and other infrastructure (Yin et al. 2016; Ortiz-Zamora and Ortega-Guerrero 2010; Van Niekerk and Van der Walt 2006).

Unlike ground deformation caused by earthquakes, the subsidence caused by aquifer consolidation is slow and imperceptible on a short timescale. This type of subsidence typically follows a decline in groundwater levels and was challenging to measure before the development of InSAR (Interferometric Synthetic Aperture Radar). In 2014, the launches of the Sentinel-1 satellites by the European Space Agency provided denser orbits, shorter repeat cycles, and higher SAR resolution, making the tracking of small ground deformations easier and more reliable. The past decade has seen the rapid development of InSAR as a tool for monitoring changes in surface elevation, and it has been used worldwide to monitor land deformation caused by earthquakes (Ryder et al. 2007; Simons 2002; Burgmann 2002), sinkholes (Intrieri et al. 2015; Baer et al. 2018; Atzori et al. 2015), and landslides (Bozzano et al. 2011; Yin et al. 2010; Kiseleva et al. 2014). The development of the small baseline algorithm (SBAS) (Berardino et al. 2002; Lanari et al. 2007) also made InSAR a suitable method to monitor large-scale gradual deformation caused by groundwater extraction.

A considerable amount of literature has been published related to the application of InSAR techniques to monitor long-term ground deformation due to groundwater

✉ Jiawei Li
   jldz9@umsystem.edu

1   Department of Geological Engineering, Missouri University
   of Science and Technology, MO, Rolla, USA

extraction. The study of Dehghani et al. (2009) used InSAR to estimate a high subsidence rate caused by overextraction of groundwater in Neyshabour, Northeast Iran. Smith et al. (2017) estimated the permanent (inelastic) subsidence that occurred from 2007 to 2010 in the San Joaquin Valley, California (USA), due to groundwater extraction using InSAR and hydraulic head measurements. Chaussard et al. (2014) used InSAR time series of ERS, Envisat, and ALOS SAR data to resolve ground deformation that occurred between 1992 and 2011 in the Santa Clara Valley, California. This study also characterized the hydrological properties of aquifer systems and fault zones by combining InSAR-based estimates of deformation with hydraulic head data. Chen et al. (2016) estimated aquifer storage properties assuming a time lag between hydrologic changes and observed deformation. Shirzaei et al. (2016) observed the link between wastewater injection and land surface uplift that caused an earthquake in eastern Texas (USA) using the InSAR technique. Teatini et al. (2012) estimated the long-term subsidence in the Venice Lagoon (Italy) using a persistent scattered SAR method with the assistance of artificial square trihedral corner reflectors (TCRs).

Although extensive research has been carried out on the feasibility of monitoring the subsidence caused by groundwater extraction using InSAR data, relatively few studies have had the data necessary to evaluate the interrelationships of geologic, hydrologic, and climate drivers on land subsidence, particularly in regions experiencing both elastic and inelastic deformation, which is complex and challenging to model. This study investigates the subsidence observed in Parowan Valley, Utah (USA), and comprehensively analyzes the spatio-temporal mechanisms of the subsidence based on InSAR data, hydrogeology, hydraulic head, precipitation, and annual water pumping.

Background

The link between hydraulic head and ground deformation in confined aquifers

A confined aquifer can be defined as an aquifer where the head at the top of the aquifer is greater than the elevation at the top of the aquifer. Confined aquifers are recharged by an upgradient source and are pressurized due to the restriction of upward flow by an overlying low-permeability unit (Fetter 2018). Figure 1 shows a simplified model of a confined aquifer of unconsolidated sediment that is common in basins such as Parowan Valley, including the fine-grained aquitards bounding the aquifer above and below, and lenses of fine-grained aquitard material, within a high-permeability coarse-grained aquifer.
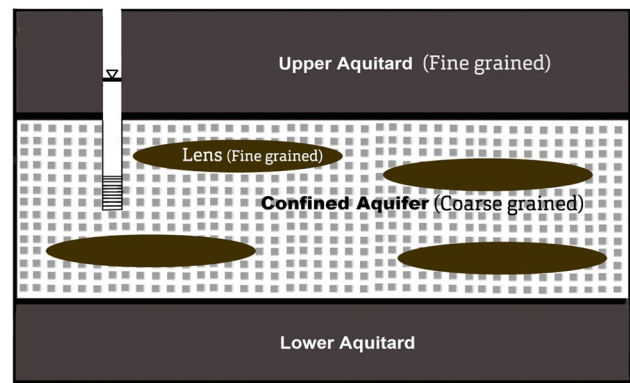
Fig. 1 A simplified model of a confined aquifer. The aquitards and lenses are fine-grained soil, and the aquifer is coarse-grained soil

For InSAR-based studies of ground deformation caused by groundwater pumping, it is assumed that the change of ground elevation measured by satellite is due to the change in thickness of the entire aquifer system (aquifers and aquitards). This change in thickness is related to the decrease or increase of hydraulic head in the aquifer and can often be correlated to groundwater extraction or recharge.

Storativity is used to describe the volume of water that can be removed from or observed by an aquifer per unit surface area per change in head. In confined aquifer systems, where the aquifer remains fully saturated during pumping, the specific storage S_s of the aquifer is defined as the volume of water released from storage from a unit volume of aquifer per unit decline in hydraulic head Fetter 2018). Jacob (1940) defined specific storage by the following equation:

$$S_s = \rho_w g(\alpha + n\beta) \tag{1}$$

where α is the compressibility of the sediment in the aquifer system, n is the porosity, β is the compressibility of water, ρ_w is the density of water, and g is gravity. This equation can be separated into two components:

$$S_s = S_{sk} + S_{sw} \tag{2}$$

where $S_{sk} = \rho_w g\alpha$ is the skeletal specific storage which corresponds to the compression of the aquifer matrix, and $S_{sw} = \rho_w gn\beta$ corresponds to the water release due to the expansion of pore water as the pressure head is reduced in the aquifer. S_{sk} is usually much greater than S_{sw}, and it can be used to estimate the change in the aquifer thickness Δb due to changes in head Δh:

$$S_{sk} = \frac{\Delta b}{b_0 \Delta h} \tag{3}$$

where b_0 is the original thickness of the stratum layer, also known as the saturated thickness.

Ground deformation caused by changing aquifer thickness could be elastic or inelastic, depending on the history

of the aquifer. Effective stress σ_e, or the difference between the total stress σ_T experienced by a geologic unit and the pore pressure P_p within the unit (Terzaghi 1925), helps to determine whether deformation is elastic or inelastic. Elastic deformation caused by increases in effective stress can be recovered when the effective stress decreases, while inelastic deformation caused by rearrangement of the grains at the pore scale in the aquifer system is typically permanent. The boundary between elastic and inelastic deformation is controlled by the historic maximum effective stress σ_{emax} (Poland et al. 1975). It is assumed that the deformation is elastic when σ_e is smaller than σ_{emax}, and deformation will become inelastic when σ_e is greater than σ_{emax}. If the main factor controlling effective stress is the change in head (as opposed to overconsolidation from glaciers or other types of loading), the head corresponding to σ_{emax} can be referred to as the preconsolidation head h_p. When head is higher than the preconsolidation head the deformation will be assumed to be elastic, and when the head is lower than the preconsolidation head the deformation will be assumed to be inelastic. Based on this theory, one can divide S_{sk} into $S_{sk} = S_{skv} + S_{ske}$ where S_{skv} is the inelastic skeletal-specific storage and S_{ske} is the elastic skeletal specific storage. Equation (3) can be rewritten for the skeletal-specific storage due to inelastic deformation as:

$$S_{skv} = \frac{\Delta b_v}{b_{0v} \Delta h_v} \qquad (4)$$

where Δb_v is the inelastic portion of the deformation, b_{0v} is the thickness of material that experienced inelastic deformation, and Δh_v is the drop in head below the preconsolidation head h_p. Similarly, the skeletal specific storage due to elastic deformation can be written as:

$$S_{ske} = \frac{\Delta b_e}{b_{0e} \Delta h_e} \qquad (5)$$

where Δb_e is the elastic portion of the deformation, b_{0e} is the thickness of material that experienced elastic deformation, and Δh_e is the drop in head above the preconsolidation head h_p. There are significant differences in the magnitude of specific storage for unconsolidated aquifers experiencing elastic and inelastic deformation. The inelastic skeletal specific storage S_{skv} is estimated to be 10–100 times larger than elastic skeletal specific storage S_{ske} (Faunt et al. 2009; Riley 1998; Sneed 2001), which means that when the hydraulic head decreases, the change in thickness of the aquifer system that is experiencing inelastic deformation Δb_v will be 10–100 times larger than the change in thickness of the aquifer system that is experiencing elastic deformation Δb_e.

The time needed for deformation to occur after groundwater has been extracted varies based on the sediment type.

Coarse-grained units typically respond quickly to changes in pore pressure within an aquifer, so consolidation in these materials tends to occur quickly, although these units are usually less compressible than fine-grained units and generally are less susceptible to consolidation. Fine-grained material like clay often has a time lag between changes in pore pressure and consolidation.

The time needed for a hydrologic unit to equilibrate to a change in head outside the unit, expressed as τ, can be approximated by the following equation when there is a step decrease in hydraulic head of equal magnitude on both the upper and lower boundaries of the unit (Riley 1969; Scott 1963):

$$\tau \simeq \left(\frac{b_0}{2}\right)^2 S_s / K_v \qquad (6)$$

where b_0 is the thickness of the equilibrated hydrologic unit. S_s is the specific storage, and K_v is the vertical hydraulic conductivity. This equation shows that fine-grained units within a coarse-grained aquifer may still experience consolidation for some time after drawdown has occurred, and the time between drawdown and consolidation will depend on the thickness, hydraulic conductivity, and specific storage of the unit. As mentioned earlier, S_{skv} is estimated to be 10–100 times larger than S_{ske}; hence, the time needed for fine-grained units to reach equilibrium will also vary depending on whether the deformation is inelastic or elastic. The delayed inelastic deformation will result in small to no seasonal uplift (rebound) during the periods of groundwater level recovery, followed by accelerated consolidation during the periods of drawdown (Riley 1969; Helm 1975).

Study area

Hydrogeology of the study area

Parowan Valley is an agricultural region in northeastern Iron County, Utah (Powell 1994), in the Basin and Range physiographic province. Parowan Valley is approximately 50 km long and 2–11 km wide and is situated in a closed surface-water basin which is the structural depression formed by northwest-trending faults (Marston 2017). The playa surface in Parowan Valley formed due to uplift along the Red-Hills fault and blockage of the Parowan Gap with alluvial-fan sediments (Anderson and Christenson 1989). Previous research done by DuRoss and Kirby (2004) indicated the existence of interbedded clay, sand, and gravel along western Parowan Valley close to the Little Salt Lake. Sand and gravel layers can be significant and may vary in thickness from a few meters near the edges of the valley to 600 m near the valley center (Fig. 2; Shah and Boyd 2018). To better understand the sediment distribution within Parowan Valley, a total of

a

b
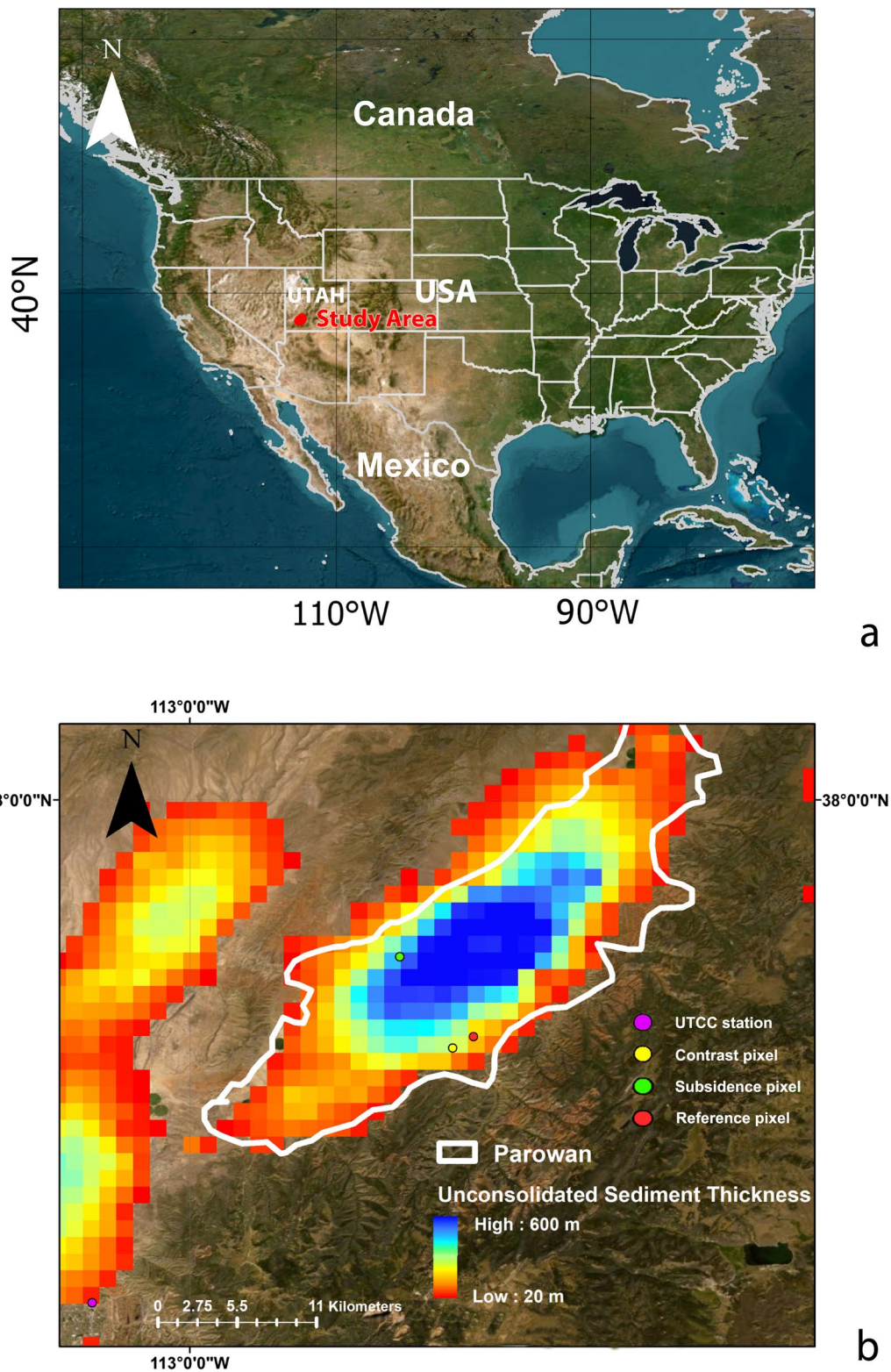
Fig. 2 **a** Location of the study area in south-western Utah. **b** The unconsolidated sediment thickness, varying from 20 to 600 m from the edge to the center of Parowan Valley (data source: Shah and Boyd 2018)

300 drillers' logs were processed. Drillers' logs were collected from different companies within a 150-year time frame, and the format and quality of the lithologic description varies considerably across the dataset. To interpret these well logs, the lithology was classified into three different categories: fine-grained, coarse-grained and mixed-grain-sized material (Table 1).

A subset of the drillers' logs was used to generate two cross-sections across the Parowan Valley using the same classification method. These cross-sections show interbedding features of fine-grained and coarse-grained material (Fig. 3). The cross-sections agree with the research done by Marston (2017), which noted that interbedding of the clay and gravel layers was observed in most of the wells across Parowan Valley. Note that since the cross-sections are based on limited lithologic information from drillers' logs, which are known to have some inconsistencies, the cross-sections are mainly useful in highlighting general geologic trends, rather than exact locations or depths of specific units. The general trend of coarse-grained sediments near the alluvial fan on the southeast portion of the valley is consistent with known geologic processes.

Recharge to the Parowan Valley aquifer is largely driven by topography-controlled precipitation and permeable sediments which allow precipitation to infiltrate. The higher elevations to the northeast, southeast, and along the eastern flank of the valley (the Markagunt Plateau and surrounding highlands) receive much more precipitation than the valley, and the sediments in these areas are of generally higher permeability, such as alluvial fans (Marston 2017). There has been a limited number of aquifer tests in the valley. Tests conducted during 1974–1975 (Bjorklund et al. 1978) show a range of hydraulic conductivity in northern Parowan Valley, of 145–213 m/day, and aquifer tests near the center of the valley (Bjorklund et al. 1978) showed hydraulic conductivities ranging from 6 to 11 m/day. Marston (2017) performed a basin characterization model (BCM) to model recharge to the aquifer, and this study found that most natural recharge to the aquifer (12.1 million m^3) comes from these highland areas, and recharge from precipitation within the valley was negligible due to lower precipitation (caused by the lower topography) and less permeable sediments. Other recharge to the Parowan aquifer comes from streambed leakage (1.6 million m^3/year), irrigation return from surface water (5.4 million m^3/year), and irrigation return from groundwater (2 million m^3/year). As these values show, the majority of recharge comes from the natural recharge from the highland areas surrounding the valley.

The aquifer tests performed in Parowan Valley show storativity ranging from 0.0007 to 0.014 with an average of 0.008683 in the northern portion of the valley and a range of 0.00007–0.02 with an average of 0.003171 in the central portion of the valley. While the storativity in the central portion of the valley is indicative of a confined aquifer, the higher storativity in the northern portion of the valley may indicate a leaky confined aquifer which may allow some recharge to occur. These results are in accordance with the BCM study performed by Marston (2017) and match the observed groundwater flow directions; groundwater flow is primarily from the northeast towards the southwest in the northern half of the valley, while a SE–NW groundwater flow component is added in the southern half of the valley. A potentiometric contour map is shown in Fig. 4, using data acquired by Marston (2017).

These results also agree with the lithologic distribution shown in Figs. 2 and 3. The increase in fine-grained layers towards the center and northwest portion of the valley is consistent with confining conditions observed in those portions of the valley (Marston 2017; Bjorklund et al. 1978). In earlier times, the Little Salt Lake likely covered a much larger portion of the valley, due to the historically wetter climate (Oviatt 1997). The confining unit may have been deposited historically from lake sediment of Little Salt Lake which is situated at the northwestern edge of the Parowan Valley. Those fine-grained deposits from the Little Salt Lake would potentially serve as the confining unit near the center of Parowan Valley.

In 2014, the Utah Geological Survey discovered a 0.25-m subsidence feature associated with fissures that developed in the Cedar Valley, just southwest of the study area. The subsidence in Cedar Valley is believed to be due to long-term overextraction of groundwater. This discovery helped promote the implementation of the water management plan in Cedar Valley to reduce the land subsidence rate (Knudsen et al. 2014). Similar fissures and ground cracks developed at the eastern end of Parowan Gap and the western margin of the Little Salt Lake playa and have been active since at least 1995. Due to surface-water flow and subsurface piping, the cracks eroded to form a significant depression up to about 1 m deep and 0.5 m wide. Localized areas of subsidence along the western margin of the Little Salt Lake playa have been observed, and water levels in Parowan Valley have dropped 6–15 m since the early 1960s (Marston 2017). However, there is limited information about the extent and magnitude of land subsidence in Parowan Valley. According to research done by Forster (2006), Parowan had less than 2.8 cm of subsidence from 1993 to 1996, and more subsidence happened from 1996 to 1998 with no specific amount mentioned.

Climate and agriculture in Parowan Valley

The climate in Parowan Valley is cold and semiarid with hot dry summers and cold winters. Parowan receives an average of 450 mm precipitation per year. Data provided by the United States Department of Agriculture (USDA) show that the most common crop grown in the Parowan area is alfalfa (Fig. 5), which generally has higher seasonal water use compared to other crops (Rogers et al. 2015). The production

Table 1 Classification of reported lithology in well logs

Classification	Types of material
Fine-grained material	Clay, mix of clay-sand; Silt, mix of silt-sand; Mix of clay-silt-sand
Mixed-grain-sized material	Mix of clay-sand-gravel; Mix of silt-sand-gravel
Coarse-grained material	Sand, mix of sand-gravel; Gravel; Mix of gravel-cobbles-boulders

of alfalfa requires considerable irrigation and has resulted in a net negative water balance over time in Parowan Valley. Some of the irrigation water in Parowan Valley comes from surface water, but most is supplied from groundwater (Marston 2017). The average estimated discharge from wells for irrigation in Parowan Valley from 1994 to 2013 is 39.7 million m^3; comparison of the groundwater discharge for irrigation with the total groundwater recharge (21.1 million m^3) shows an average water deficit. The continuous over-withdrawal of groundwater from 1974 to 2013 has caused the groundwater level to decline by up to 9 m in the northern portion of the valley and by up to 27 m in the central portion of the valley (Marston 2017). Lack of precipitation during a drought year could cause additional stress to the aquifer due to limited surface water supplies and higher water demand during the growing season, which could result in more rapid declines.

Methods

InSAR data acquisition and processing

Interferometric Synthetic Aperture Radar (InSAR) is a technique for measuring surface deformation using the difference in the phase of microwave electromagnetic waves in two or more SAR images. InSAR is sensitive to ground deformation on the order of millimeters or centimeters (Massonnet and Feigl 1998). InSAR data over the study area were processed using GMTSAR software developed by David Sandwell and Xiaohua Xu (Sandwell et al. 2011). The Small Baseline Subset (SBAS; Berardino et al. 2002) method was used to generate the InSAR time series and mean ground displacement velocity map. For InSAR analysis of Parowan Valley, a total of 155 descending SAR scenes from the Alaska Satellite Facility (ASF) were used. These scenes were acquired by the Sentinel-1 satellite from 29 November 2014, to 27 December 2020 (Path 100, Frame 464 and 465 for 2014–2016, Frame 466 for 2017–2020) with a 12-day time interval between adjacent passes. A total of 404 interferograms were generated and used for time-series analysis.

Ground-displacement mean velocity map and time-series

A vertical displacement mean velocity map (land subsidence map) was generated using the SBAS method. Time series of deformation were computed relative to a reference pixel that was assumed to have very little deformation. The reference pixel was selected in an urban area in the city of Parowan, Utah (−112.829° longitude, 37.846° latitude) because of its stable reflection properties, negligible groundwater pumping in this region (Marston 2017), and because it is located on an alluvial fan with coarse-grained deposits, which deform much less than clay-rich sediments. This reference pixel has similar tropospheric patterns to the rest of the valley that has more deformation, and thus it is effective for testing the removal of most tropospheric effects.

If the tropospheric effects were removed successfully, a randomly selected pixel near the reference pixel with no significant pumping and similar geologic conditions would also have little to no subsidence. To verify that the processing method was successful in measuring subsidence and was not unduly influenced by tropospheric effects, two points were selected to extract the time series. One pixel, referred to here to as the subsidence point, was in a high-subsidence area (−112.869° longitude, 37.902° latitude) to measure the accumulated subsidence from 2014 to 2020. Another pixel, referred to as the contrast point, was in an urban area similar to the reference pixel (−112.836° longitude, 37.845° latitude) to corroborate the successful removal of the atmospheric noise, The locations of these pixels are marked in Fig. 2. To further validate the InSAR data, a global positioning system (GPS) station (UTCC) close to southeastern Parowan Valley (Fig. 2) was used to compare with the InSAR data at the same location. Results indicate similar elevation trends with time between the InSAR and GPS data (Fig. 6a).

Results and discussion

Temporal comparison of hydraulic head and subsidence

The maximum subsidence in Parowan Valley calculated from the InSAR time series is 26.2 cm over the 6-year study period. Groundwater levels from a United States Geological Survey (USGS) monitoring well shown in Fig. 6b located in the center of Parowan Valley (in the subsiding region, shown in Fig. 7a), indicate that between 2014 and 2020, the head in this area dropped by approximately 3 m.

Figure 6c shows the maximum ground deformation observed each year (maximum ground elevation–minimum ground elevation) as a function of the change in head for each year. The expected trend of increasing subsidence with
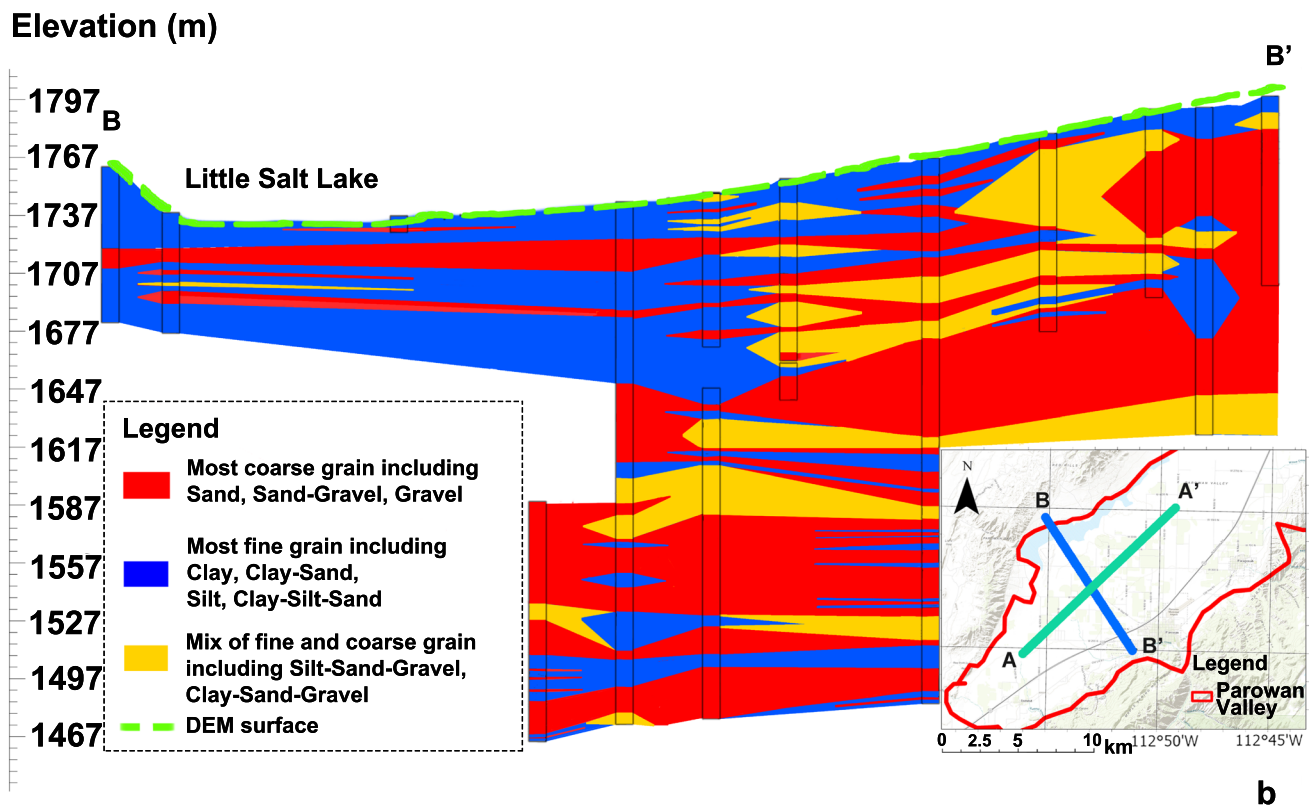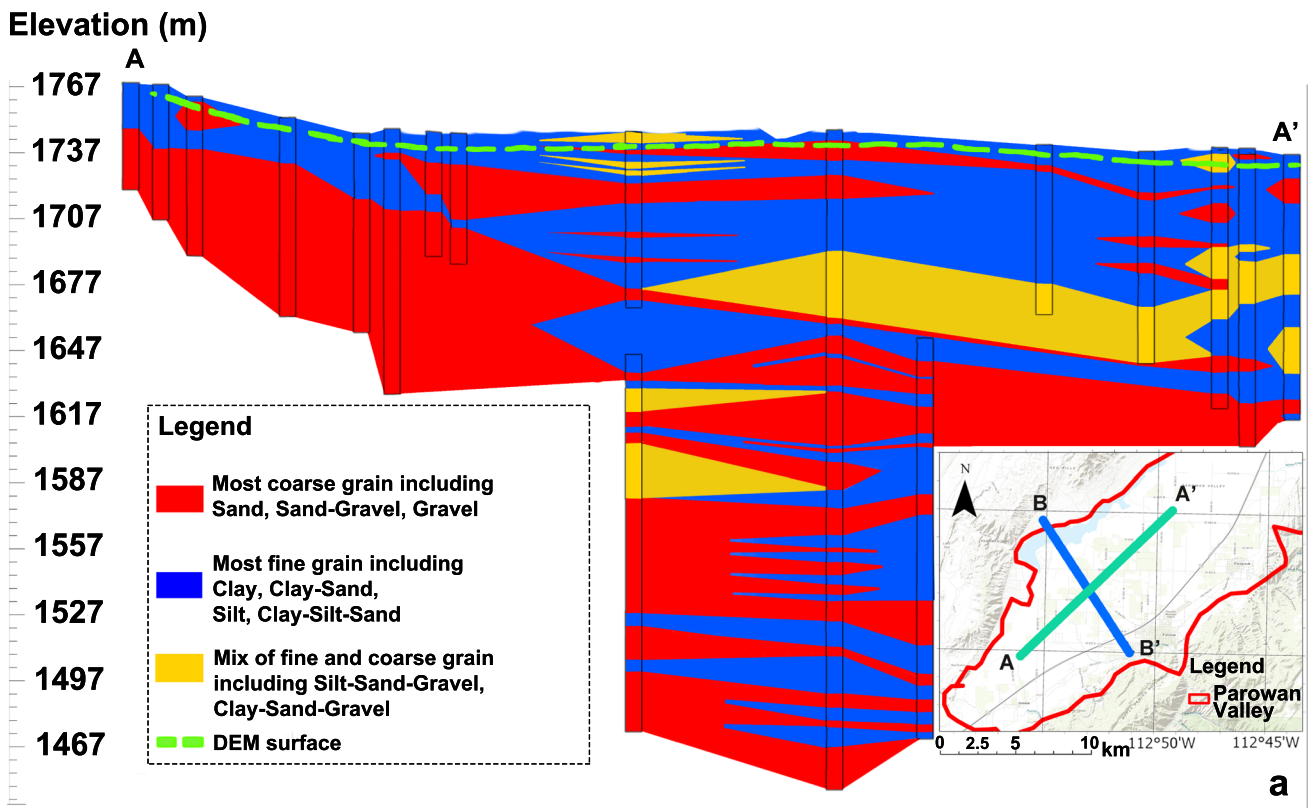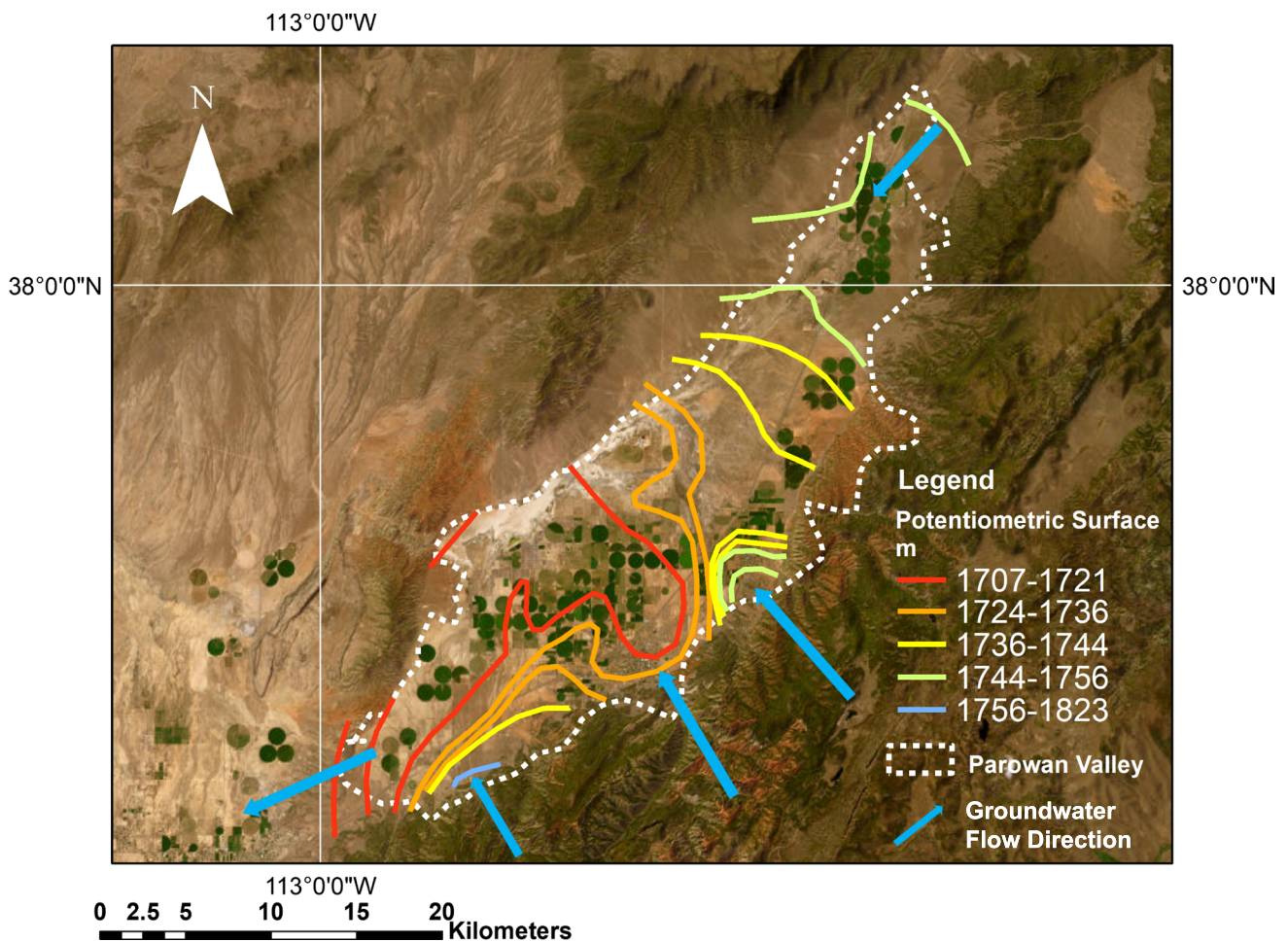
Fig. 3 Interpreted cross-sections based on drillers' logs. **a** Cross-section in the southwest–northeast direction along the Parowan Valley marked as AA'. **b** cross-section in the northwest–southeast direction across the Parowan valley marked as BB'

Fig. 4 The potentiometric surface, modified from Marston (2017), showing groundwater recharge from the northeastern and southeastern parts of Parowan Valley. This potentiometric surface was based on the head measurements in 2013

decreasing head is observed, but there is not a simple linear correlation between these two variables. The scatter in this graph is probably due to a time delay in subsidence from when the head drop first occurs due to the delayed response of fine-grained units, but the time delay cannot be adequately characterized using the limited number of head measurements available (one head measurement per year).

As explained in section 'The link between hydraulic head and ground deformation in confined aquifers', ground subsidence and elastic rebound may have a delayed response to the lowering or raising of the hydraulic head in the aquifer due to the low hydraulic conductivity of the fine-grained units within the aquifer. After a large decrease in hydraulic head, subsidence could continue for years to decades as the hydraulic head comes to equilibrium in fine-grained units. The measurement in the monitoring well was taken in March of each year, which generally has the highest head levels of the year; hence, the actual head would be lower around

December, which is the time when peak subsidence measurements usually occur.

There is evidence of both long-term (likely inelastic) and short-term (a significant component of which is elastic) signals in the deformation data. Longer-term subsidence is shown by the occurrence of subsidence even during periods of increasing head, which indicates subsidence resulting from the decrease in head in previous years. Short-term subsidence (within 1 year) is shown by high subsidence rate in the years with high head drop. In addition, Figure 6b shows that the ground rebounds after subsidence from approximately October to March of the following year, indicating that some compressible materials are rapidly expanding elastically after the recovery of heads. The occurrence of subsidence in years where the head increases, as well as the greater magnitude of subsidence relative to rebound, indicate that there is significant inelastic deformation occurring. More detail on the relationship between head, elastic deformation,
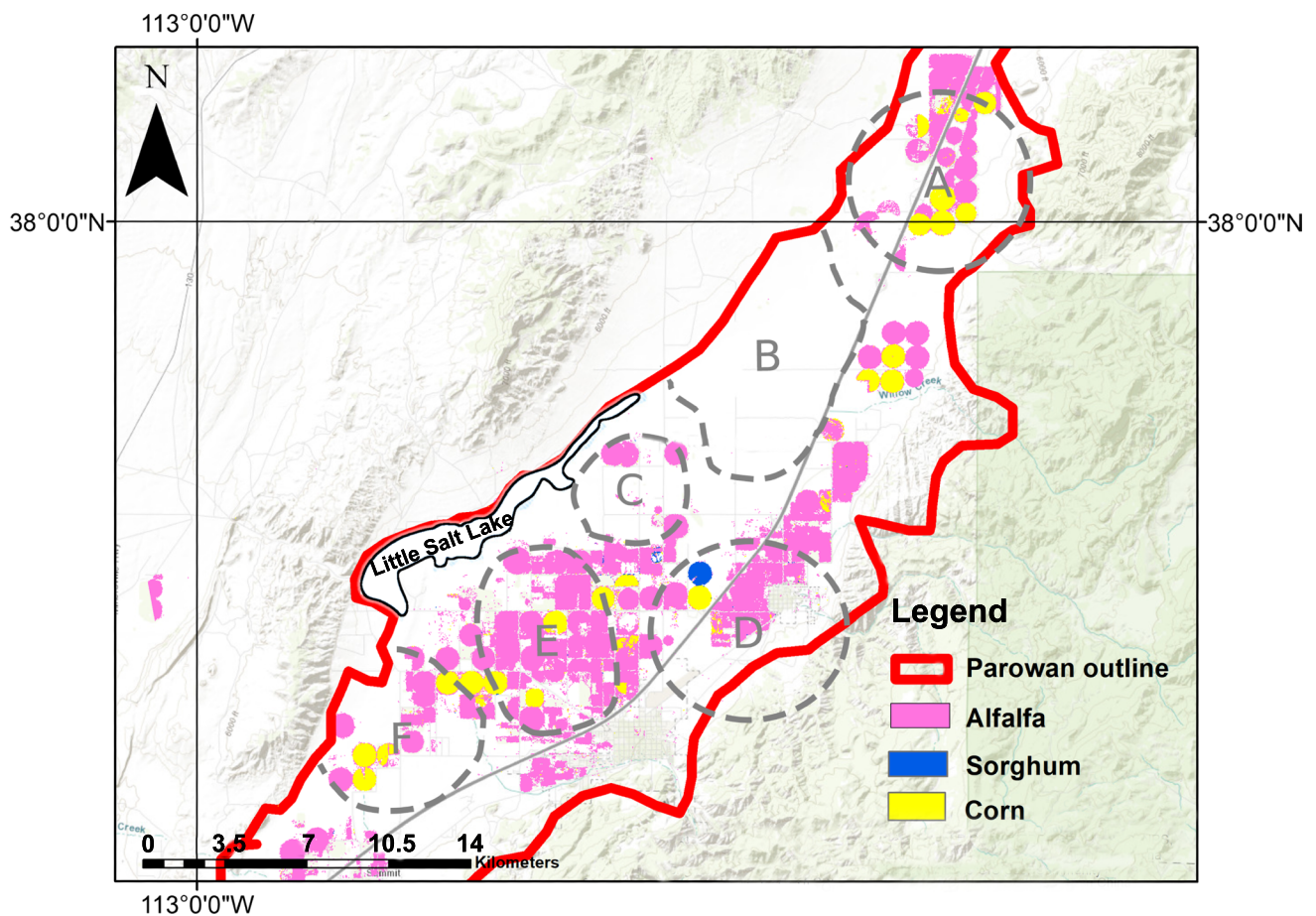
Fig. 5 Major crop types grown in Parowan Valley, from the Cropland Data Layer (Boryan et al. 2011)

inelastic deformation, and delayed subsidence in Parowan Valley are discussed in Smith and Li (2021).

### The relationship between lithology, subsidence, and drawdown

The lithology distribution map, which was created based on the well logs across Parowan Valley, indicated the existence of extensive fine-grained materials. These fine-grained units, as well as the mix of clay-silt-sand material in the center of the Parowan Valley, are liable to consolidate when the head is decreased, and thus subsidence is most likely to occur over these units. The northwestern part of the lithology distribution map marked as region B in Fig. 7 was interpreted because no well logs were present in this area.

The mean subsidence velocity map indicated that a maximum of 5.3 cm/year subsidence happened in the Parowan Valley (Fig. 7a) over the period 2015–2020, with major subsidence at the center of the valley close to the Little Salt Lake region. The contour lines shown in Fig. 7a were generated based on the subsidence mean velocity

rate and represent major subsidence areas with subsidence rates greater than 1 cm/year. Overlapping the lithology distribution map and mean subsidence velocity map showed that major subsidence happened in the areas with higher percentages of fine-grained and mixed-grain-sized (>50% fines) materials, while areas that contained more coarse-grained material had limited ground deformation (Fig. 7b).

The drawdown map (Fig. 7c) was created based on USGS monitoring wells data from 2015 to 2021 (the head measurement was in March each year). The map shows more than 4 m of drawdown in the southwestern portions of the valley, 2–3 m drawdown in the central valley, and close to 3-m drawdown in the northern valley. The area shaded grey has a lack of data.

Visual comparison of the Fig. 7a–c parts shows that, in general, subsidence was greater in areas with more fine-grained materials and higher drawdown. The contour lines of subsidence also fit the boundary of the lithology map in the central Parowan Valley where the apparent change of lithology occurs as shown in Fig. 7b.
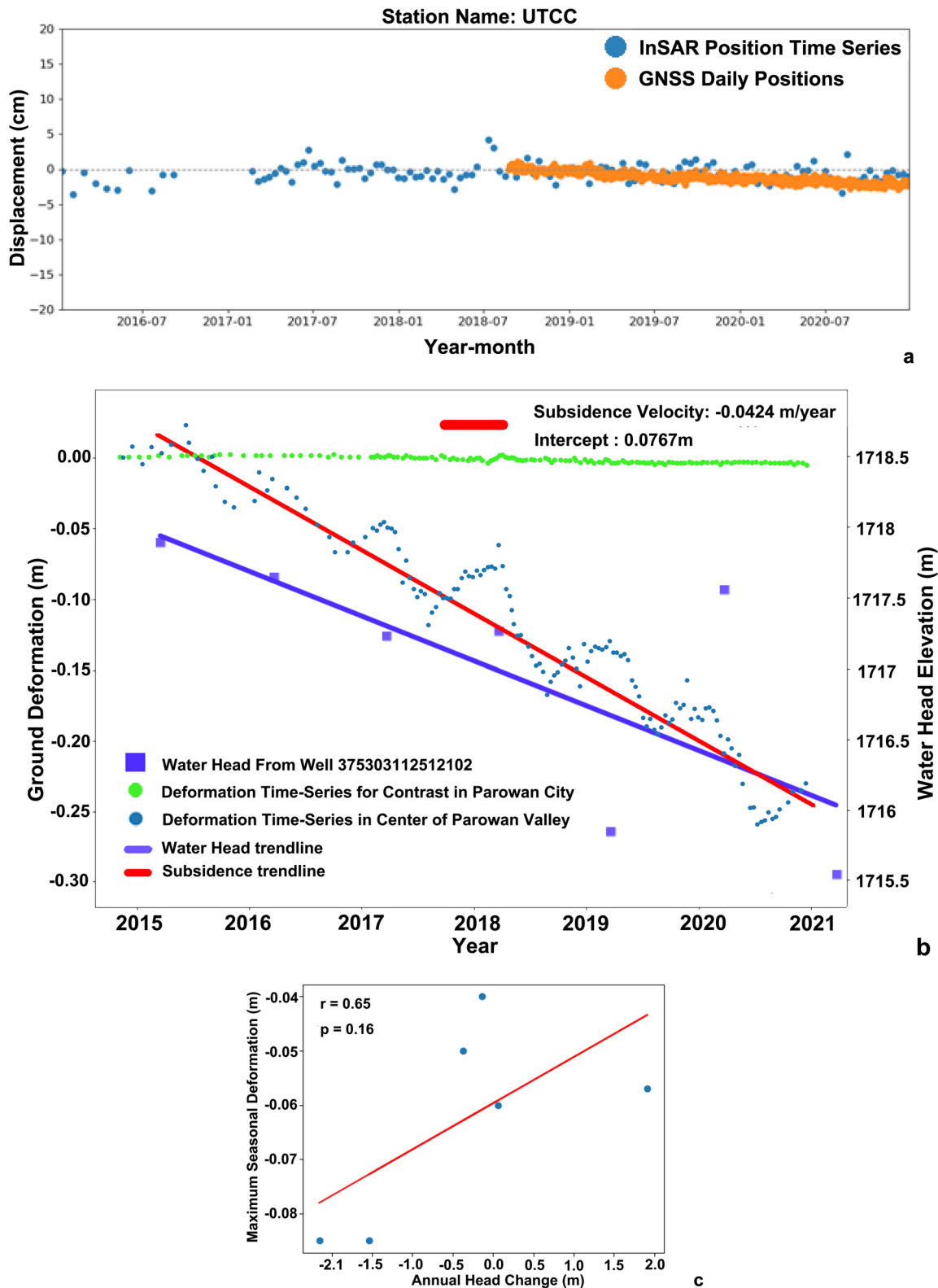
Fig. 6 a Comparison between InSAR and GNSS data, **b** Ground deformation data measured with InSAR from the subsidence pixel and water level (head) from the monitoring well closest to the sub-sidence pixel, locations were marked in Fig. 7a. **c** Relation between maximum seasonal deformation and annual head change

The relationship between subsidence and precipitation

A weather station was installed at Yankee Reservoir located southeast of Parowan Valley, in the mountains that source most of the surface water that Parowan Valley receives, to record the annual precipitation (snow and rain). The annual precipitation was compared with the annual subsidence data, shown in Fig. 8. The annual subsidence data shown are from the subsidence pixel (see Fig. 7a). The lowest subsidence level in the time series for each year was used to calculate the annual subsidence. This point is used as an example to illustrate the relation between subsidence and precipitation, but the relationship between precipitation and subsidence likely varies regionally throughout the valley. In 2018 and 2020, the precipitation in Parowan was less than 400 mm, which is around 40% less than the average precipitation, and the subsidence during these years was higher than in the other years of this study. Although precipitation does not directly recharge the aquifer in a short range of time, high precipitation in the valley during the growing season will result in surface-water availability that meets or partially meets irrigation water demand and thus leads to lower groundwater extraction. Low precipitation will increase groundwater extraction for irrigation needs and causes stress to the aquifer. As noted in section 'Temporal comparison of hydraulic head and subsidence' and Fig. 6b, even periods with high precipitation and increases in hydraulic head (2017, 2019) have significant subsidence, likely due to the delayed response of the low-permeability clay layers to previous declines in hydraulic head.

Discussion on the ground deformation mechanism in Parowan Valley

In this study, InSAR, lithology, hydraulic head, drawdown, and precipitation data in Parowan Valley were compared, and some visual correlations between these factors and subsidence were identified, as shown by areas with higher subsidence in areas with more fine-grained materials and higher drawdown. However, the mechanisms of subsidence are more complex, with this research indicating that ground subsidence caused by groundwater extraction is driven by multiple parameters including drawdown, agricultural activity, precipitation, groundwater gradient, and aquifer conditions, which will be discussed individually in the following sections.

Drawdown

Drawdown is one key parameter in ground deformation caused by groundwater extraction. Large drawdown will decrease pore pressure in the aquifer system, causing short-term aquifer consolidation and long-term aquitard dewatering. The connection between drawdown and subsidence is well illustrated, in region C marked on Fig. 7. Comparison of Fig. 7a–c shows that when lithologies in the vertical zone of pumping are similar, higher drawdown (2.46 m) led to a higher subsidence rate (−0.0199 m/year), while the well close to the high-drawdown well, with drawdown of only 0.74 m, has a subsidence rate of −0.0069 m/year. Drawdown is also driven by multiple parameters including agricultural activity, precipitation, and recharge location.

Agricultural activity affects the drawdown temporally and spatially, mainly related to when and where farmers pump groundwater for irrigation uses. As shown in Fig. 6b, the subsidence in Parowan Valley shows seasonal fluctuations, with the most subsidence happening in the growing season (May–Oct), indicating that the agricultural activity is causing the drawdown. Region B, marked in Figs. 5 and 7, was interpreted as having a higher percentage of fine-grained material, but this region has little to no subsidence due to the lack of agricultural activity and active pumping wells in this area.

Precipitation As discussed in section 'The relationship between subsidence and precipitation', precipitation will affect the subsidence rate indirectly. High precipitation in the valley during the growing season will result in surface-water availability that meets or partially meets irrigation water demand and thus leads to lower groundwater extraction and less drawdown. Low precipitation, on the other hand, will increase the groundwater extraction for irrigation needs, which can lead to increased drawdown. Figure 9 compares subsidence, water head change and precipitation quantitatively, and indicates a strong positive correlation between water head change and precipitation and a strong negative correlation between subsidence and precipitation, which supports the assumption that precipitation and drawdown are related in Parowan Valley.

Recharge location Groundwater recharge will also affect the drawdown; regions close to the upgradient recharge area will more likely have less drawdown than regions further away from the recharge area. According to the pumping data for individual wells in Parowan Valley (Marston 2017), region A in Fig. 7 had total water extraction of 7.7 million m^3 in 2013, while region F had total water extraction of 3.8 million m^3. The total pumping in Parowan Valley in 2013 was 39.5 million m^3, which is similar to the average pumping of 44.3 million m^3 during 2015–2020. It was assumed that pumping data for individual wells in 2013 can be used to approximately represent the yearly pumping during the 2015–2020 time frame. Near region A, the aquifer experienced 7.7 million m^3 of pumping and had an average of 0.58 m yearly drawdown. Near region

Fig. 7 a Mean subsidence rate map generated using the SBAS method. Contour lines delineate the subsidence rate, revealing the areas with the highest subsidence. **b** Distribution of fine-grained and mixed-grain-sized soil in the Parowan Valley. The contour lines again show the subsidence rate during 2015–2020. **c** Drawdown (m) map of Parowan Valley using data from USGS monitoring wells. Areas A–F are described in the text. Monitoring wells marked in red represent locations that more likely experienced inelastic deformation, green represents locations that more likely experienced elastic deformation, and yellow represents locations that likely experienced a mix of elastic and inelastic deformation, more detail is described in the text
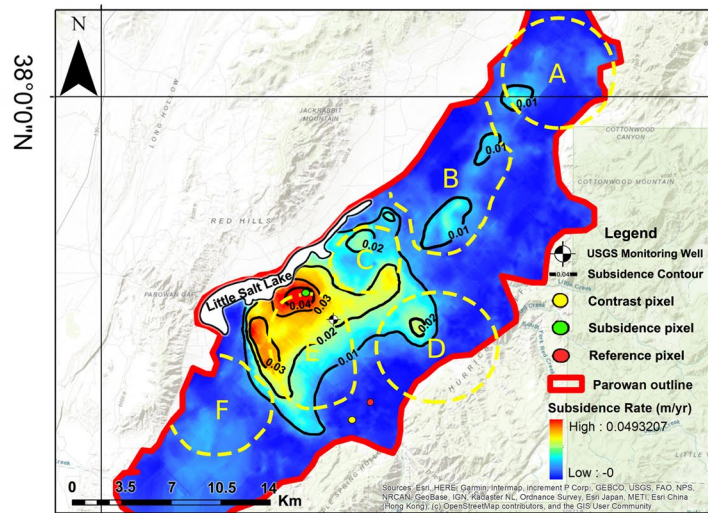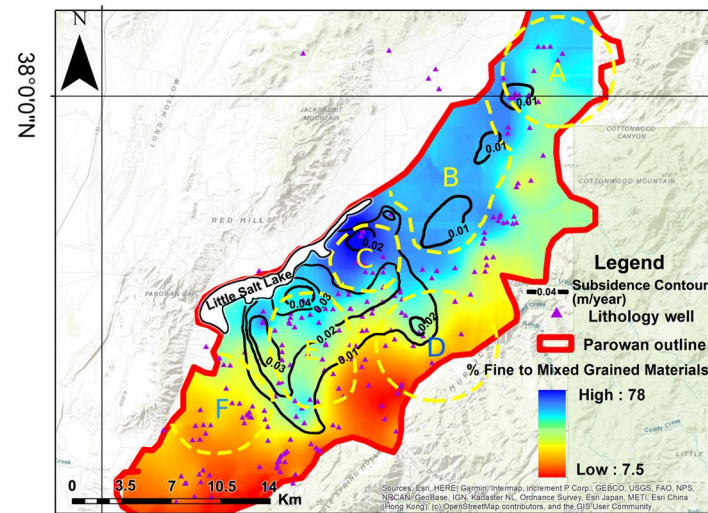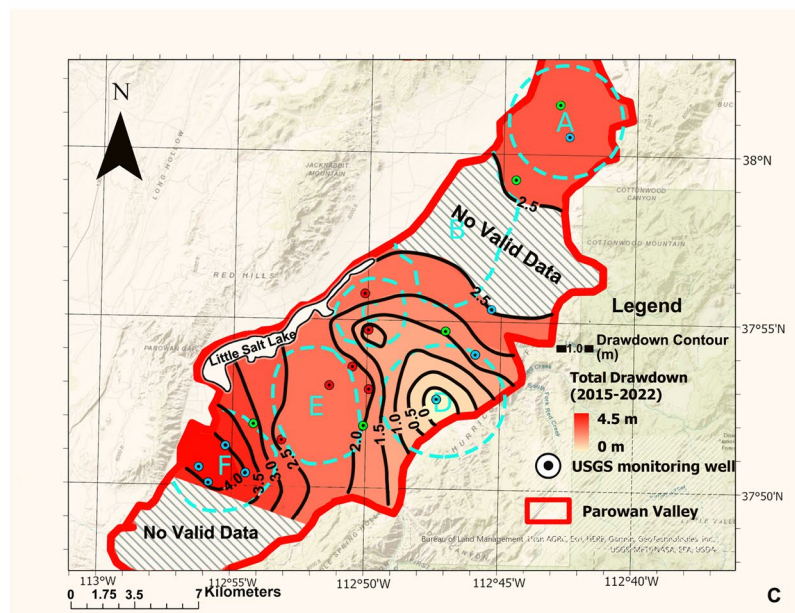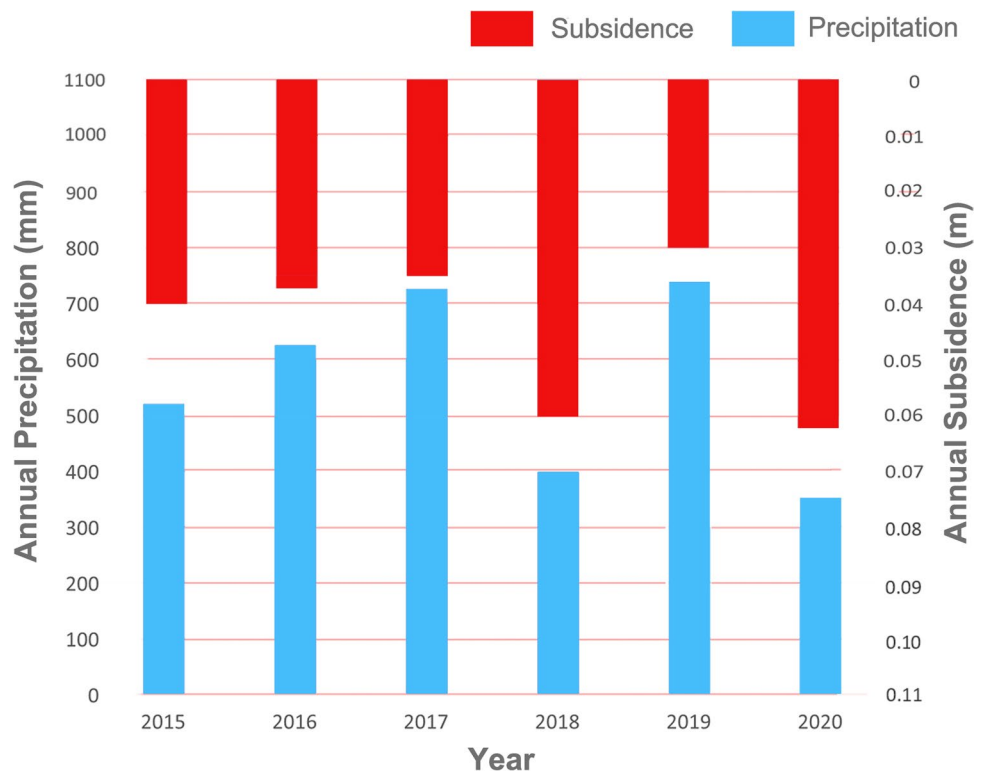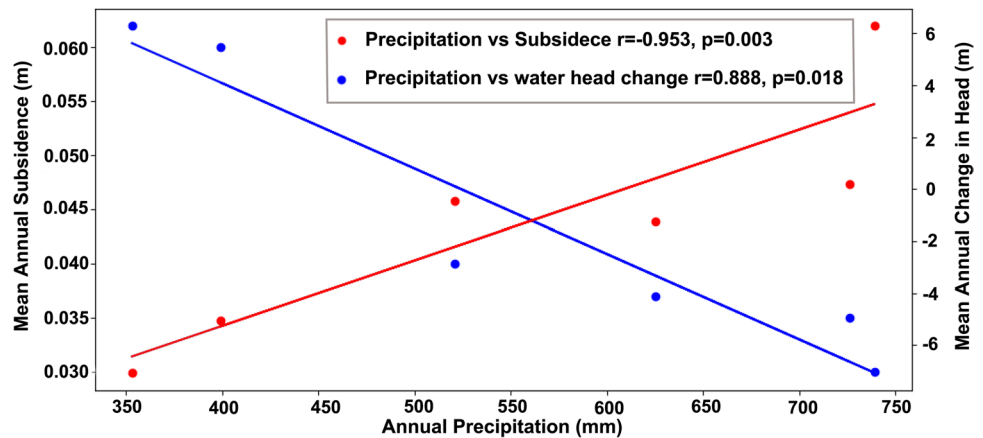
Fig. 8 Temporal relation between annual precipitation and ground subsidence. Blue bars represent annual precipitation and red bars represent annual subsidence

Fig. 9 Correlation between precipitation, subsidence, and water-head change. Negative water-head change means drawdown, while positive water-head change indicates recovery

F, the aquifer experienced 3.8 million m³ of pumping and had an average of 0.82 m yearly drawdown, indicating a difference of nearly 3× of the yearly drawdown per unit million m³ of pumping between the aquifers in the northeastern and southwestern portions of the Parowan Valley. As mentioned earlier in section 'Study area', groundwater recharge in Parowan Valley mainly happens in the northeastern, eastern, and southeastern highlands, so aquifers close to the eastern mountains in Parowan Valley typically receive recharge more quickly than aquifers in the central and southwestern Parowan Valley, which may help to explain the low drawdown in northeastern parts of the valley.

Aquifer properties

Aquifer properties are important in determining how ground deformation will occur in response to groundwater extraction. Differing amounts of deformation will occur in response to drawdown under different thicknesses of consolidating interval, in aquifers with interbedded features of fine-and-coarse-grained material and clay lenses, and in aquifers experiencing elastic and inelastic deformation.

Thickness of consolidating interval Under similar drawdown, larger consolidating thickness will generally respond with higher deformation due to the greater thickness of clay

sediment that experienced reduced pore pressures. To perform a quantitative analysis, subsidence data close to US Geological Survey monitoring wells in region E and region A were compared. In central Parowan Valley, the mean total drawdown in three monitoring wells around region E from 2015 to 2020 was 2.3 m, the average well depth is 200 m, and the mean subsidence rate corresponding to the location of monitoring wells was close to 0.018 m/year. In northern Parowan Valley, the mean total drawdown in three monitoring wells around region A from 2015 to 2020 was 2.8 m, the average well depth is 90 m, and the mean subsidence rate corresponding to the location of monitoring wells was close to 0.007 m/year. Although the drawdown in the northern Parowan Valley was higher than that of the central Parowan Valley, the subsidence rate was lower, which is likely due to the shallower well depth in the northern Valley, resulting in a lower total thickness of clay sediments experiencing pore pressure declines. Additionally, while the recent drawdown rates are similar, the historical drawdown rates of central Parowan Valley are much higher than northern Parowan Valley. The central Parowan Valley experienced roughly 27 m of drawdown from 1974 to 2013, while the northern Parowan Valley experienced roughly 15 m of drawdown over the same period (Marston 2017). Delayed subsidence in the central Parowan Valley, caused by historical declines in head, could thus also explain some of the higher-than-expected subsidence rates experienced there.

Proportion of fine-grained material As mentioned in section 'The relationship between lithology, subsidence, and drawdown', the maps of subsidence and fine-grained material percentages indicate that subsidence mainly happened in the areas where the proportions of fine-grained material were greater than 50%. To further investigate the relationship between ground deformation rate and the proportion of fine-grained material, the mean velocity

map (Fig. 7a) and lithology distribution map (Fig. 7b) were sampled with a pixel size of 114 × 114 m and quantitatively compared using a scatter plot (Fig. 10). This plot shows that not only areas with low percentages of fine-grained materials typically experience low subsidence, but also that high percentages of fine-grained materials only result in subsidence when drawdown is also an important factor. When drawdown levels were similar, no obvious subsidence trend was observed when the proportion of fine-grained material was lower than 30%, and the subsidence trend shows that, if drawdown is also significant, it will gradually increase while the proportion of fine-grained material is between 35 and 55%. Regions B and C have little to no drawdown (Fig. 7a); hence, there will be little to no deformation.

Aquifer with interbedded features and clay lenses Confined aquifers with interbedded fine-grained units within the coarse aquifer will be more likely to deform when drawdown happens than aquifers without fine-grained units. After pressure drops in the confined aquifer system, thin fine-grained units within the aquifer will dewater and reach equilibration fairly quickly, causing relatively quick deformation. In Fig. 3, cross section 1 is in the region with a similar drawdown of between 2 and 2.5 m. This cross section shows more interbedded features from the northwestern part to the central part, and this region shows a high deformation rate (0.035–0.027 m/year) in Fig. 7a between regions E and F. The southeastern part of cross section 1 shows fewer fine-grained units interbedded in the aquifer and lower deformation rate (0.02–0.001 m/year).

Elastic and inelastic deformation As mentioned in section 'The link between hydraulic head and ground deformation in confined aquifers', in confined aquifers, the deformation will be elastic when the head is above the preconsolidation head, and deformation will be inelastic when the

Fig. 10 Scatter plot between ground deformation rate and proportion of fine-grained material in the subsurface
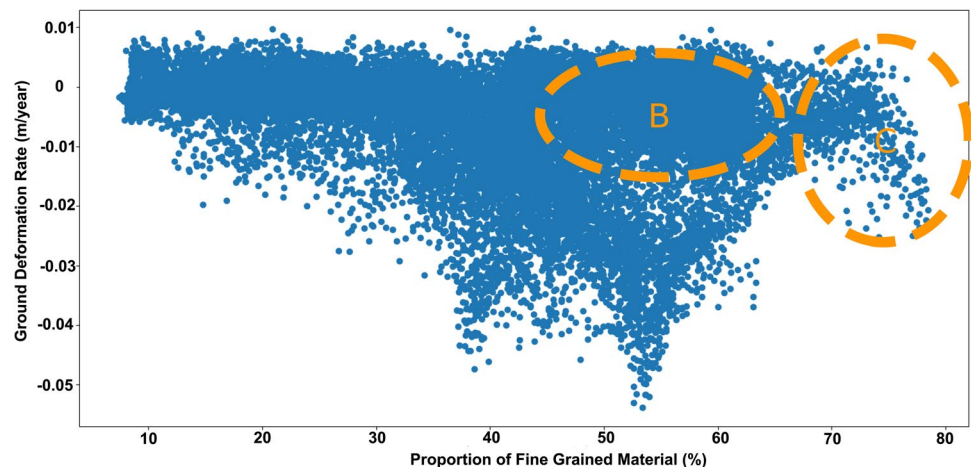
head drops below the preconsolidation head. The elastic deformation is recoverable, and the inelastic deformation is permanent. For the same change in head, inelastic deformation will be 10–100 times larger than elastic deformation due to the magnitude difference between inelastic skeletal specific storage S_{skv} and elastic skeletal specific storage S_{ske}. To examine the elastic and inelastic deformation conditions in Parowan Valley, the drawdown, well depth, and deformation rate near USGS monitoring wells in Fig. 7 were used to generate a S_{sk} cross plot using Eq. (3) (Fig. 11). This plot shows that both elastic and inelastic subsidence is occurring in Parowan Valley. To better understand the spatial distribution of elastic and inelastic subsidence, the response of individual wells was considered. The range of inelastic deformation and elastic deformation was based on S_{ske} and S_{skv} values of 6.6E-6 m^{-1} to 2.5E-5 m^{-1} and 4.6E-4 m^{-1} to 2.2E-3 m^{-1}, respectively, as provided by Sneed (2001). When the resulting S_{sk} value was greater than the typical S_{skv} value, the well was colored red in Fig. 7c as an area experiencing inelastic deformation. When the resulting
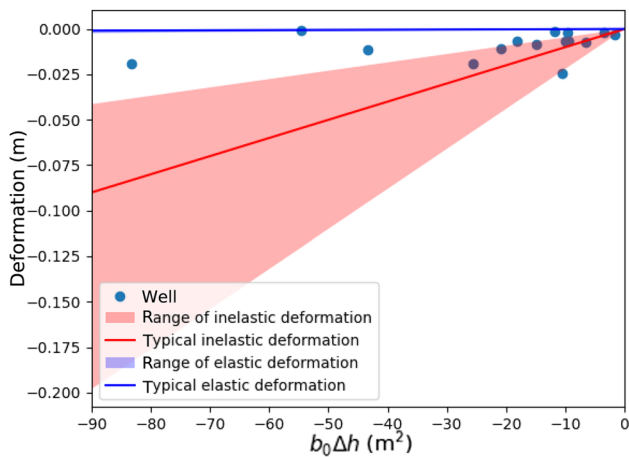
S_{sk} value was lower than the typical S_{skv} value but greater than S_{ske} values, the well was colored green in Fig. 7c as an area likely experiencing a mix of inelastic and elastic deformation. When the resulting S_{sk} value was close to S_{ske}, the well was colored blue in Fig. 7c as an area likely experiencing elastic deformation. The results show that regions in central Parowan Valley close to Little Salt Lake mostly experienced inelastic deformation, regions close to northern Parowan Valley likely experienced a combination of inelastic and elastic deformation, and regions close to southwestern Parowan Valley likely experienced elastic deformation.

Conclusion

During this research, close to 30 cm of ground deformation was measured at the center of Parowan Valley using InSAR. To examine that ground deformation, InSAR, well log lithology, hydraulic head, drawdown, groundwater pumping, groundwater recharge, agricultural, and precipitation data in Parowan Valley were analyzed. Results showed that the deformation that happened in central Parowan Valley was generally inelastic due to the overextraction of groundwater that led to a hydraulic head drop below the preconsolidation head. To further explore the mechanisms of the ground deformation, several quantitative analyses were applied between drawdown, precipitation, water head, deformation rates, and the proportion of fine-grained material. The results showed that high deformation typically occurred in areas with high drawdown, low precipitation, and low groundwater recharge. Confined aquifers with many interbedded fine-grained units and with a high proportion of fine-grained material (between 35 and 55%), and with head that dropped below the preconsolidation head, were shown to deform inelastically. Other portions of the valley typically deformed elastically, but these areas may not experience full recovery outside the growing season due to the overextraction of groundwater and insufficient aquifer recharge.

Fig. 11 Range of specific storage for all monitoring wells in Parowan Valley

Appendix A. Aquifer test in Parowan
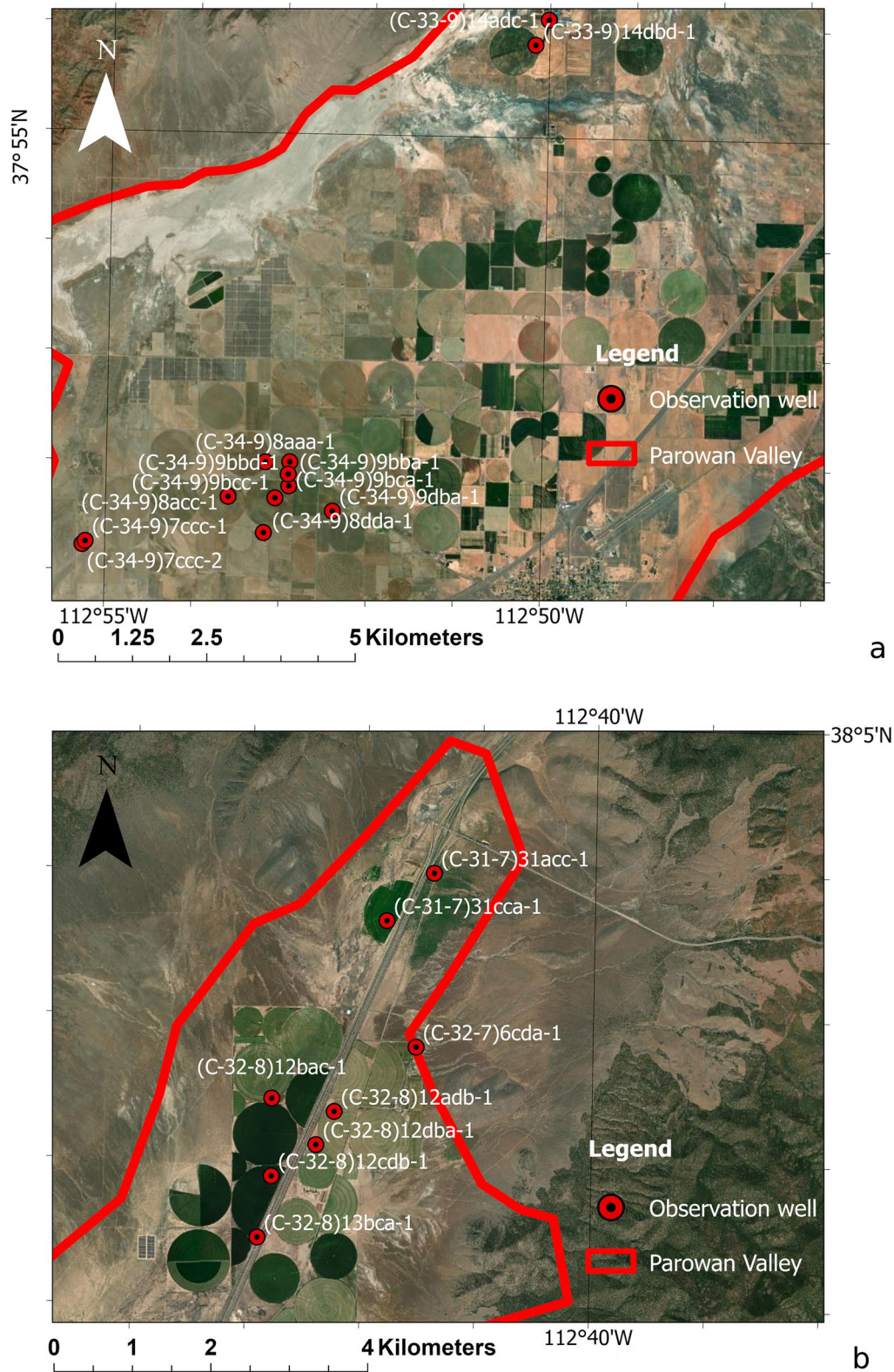
Fig. 12 Approximate locations of wells used in the aquifer test during 1974–1975 by Bjorklund et al. 1978 in Parowan Valley. **a** Observation wells in central Parowan Valley. **b** Observation wells in northern Parowan Valley

Table 2 Aquifer test results by Bjorklund et al. 1978 in Parowan Valley. T transmissivity, K hydraulic conductivity, S_s specific storage

Pumped well	Observation well	Date (and length) of test	Distance to pumped well (m)	Discharge of well (m³/min)	T (m²/day)	Average K (m/day)	S_s	Water-bearing material	Saturated section open to well (m)	Type of test	Rating of test
(C-32-8)12bac-1	–	13–31 May 1974 (430 h)	–	10	–	–	–	Volcanic debris	–	–	–
	(C-31-7)31acc-1		3,658	–	–	–	–	Gravel	7	–	–
	(C-31-7)31cca-1		2,736	–	37,719	–	0.0056	Volcanic debris	–	Drawdown	Good
	(C-32-7)6cda-1		2,044	–	62,895	–	0.0028	Volcanic debris	47	Drawdown	Good
	(C-32-8)12adb-1		933	–	17,930	145	0.011	Volcanic debris	123	Drawdown	Good
	(C-32-8)12cdb-1		927	–	18,766	213	0.0007	Volcanic debris	88	Drawdown	Good
	(C-32-8)12dba-1		918	–	9476	–	0.014	Volcanic debris	–	Drawdown	Fair
	(C-32-8)13bca-1		1,692	–	30,658	–	0.018	Volcanic debris	47	Drawdown	Good
(C-33-9)14dbd-1	–	18–31 Oct 1974 (76 h)	–	3.7	130	–	–	Gravel sand and silt	–	Recovery	Good
	(C-33-9)14adc-1		1,127.76	–	1,022	11	0.02	Gravel sand and silt	91	Recovery	Poor
(C-34-9)7ccc-2	–	31 July–2 Aug 1973 (17 h)	–	2.2	–	–	–	Gravel	–	–	–
	(C-34-9)7ccc-1		29	–	585	8	0.00007	Gravel	75	Recovery	Good
(C-34-9)9bca-1	–	25–27 Mar 1975 (50 h)	–	5	–	–	–	Gravel	171	–	–
	(C-34-9)8aaa-1		671	–	1,663	11	0.003	Gravel	185	Drawdown	Good
	(C-34-9)8acc-1		1,189	–	–	–	–	Gravel	–	Drawdown	Poor
	(C-34-9)8dda-1		792	–	845	11	0.0006	Gravel	75	Drawdown	Good
	(C-34-9)9bba-1		625	–	1,245	6	0.0005	Gravel	202	Drawdown	Good
	(C-34-9)9bbd-1		183	–	560	8	0.0003	Gravel	71	Drawdown	Good
	(C-34-9)9bcc-1		320	–	829	10	0.0004	Gravel	85	Drawdown	Good
	(C-34-9)9dba-1		793	–	1,050	6	0.0005	Gravel	195	Drawdown	Fair

Declarations

Conflict of interest On behalf of all authors, the corresponding author states that there is no conflict of interest.

References

Anderson RE, Christenson GE (1989) Quaternary faults, folds, and selected volcanic features in the Cedar City 1°×2° quadrangle, Utah. Utah Geological and Mineral Survey, Salt Lake City, UT

Anzidei M, Bosman A, Carluccio R, Casalbore D, D'Ajello Caracciolo F, et al (2017) Flooding scenarios due to land subsidence and sea-level rise: a case study for Lipari Island (Italy). Terra Nova 29(1):44–51. https://doi.org/10.1111/ter.12246

Atzori S, Baer G, Antonioli A, Salvi S (2015) InSAR-based modeling and analysis of sinkholes along the Dead Sea coastline. Geophys Res Lett 42(20):8383–8390. https://doi.org/10.1002/2015gl066053

Baer G, Magen Y, Nof RN, Raz E, Lyakhovsky V, Shalev E (2018) InSAR measurements and viscoelastic modeling of sinkhole precursory subsidence: implications for sinkhole formation, early warning, and sediment properties. J Geophys Res: Earth Surf 123(4):678–693. https://doi.org/10.1002/2017jf004594

Berardino P, Fornaro G, Lanari R, Sansosti E (2002) A new algorithm for surface deformation monitoring based on small baseline differential SAR interferograms. IEEE Trans Geosci Remote Sens 40(11):2375–2383

Bjorklund LJ, Sumsion CT, Sandberg GW (1978) Ground-water resources of the Parowan-Cedar City drainage basin, Iron County, Utah. Technical Publ. no. 60, Utah Department of Natural Resources, Salt Lake City, UT, 93 pp

Boryan C, Yang Z, Mueller R, Craig M (2011) Monitoring US agriculture: the US Department of Agriculture, National Agricultural Statistics Service, Cropland Data Layer Program. Geocarto Int 26(5):341–358

Bouwer H (1977) Land subsidence and cracking due to ground-water depletion. Groundwater 15:358–364. https://doi.org/10.1111/j.1745-6584.1977.tb03180.x

Bozzano F, Cipriani I, Mazzanti P, Prestininzi A (2011) Displacement patterns of a landslide affected by human activities: insights from ground-based InSAR monitoring. Nat Hazards 59(3):1377–1396

Burgmann R (2002) Deformation during the 12 November 1999 Duzce, Turkey, earthquake, from GPS and InSAR data. Bull Seismol Soc Am 92(1):161–171. https://doi.org/10.1785/0120000834

Chen J, Knight R, Zebker HA, Schreüder WA (2016) Confined aquifer head measurements and storage properties in the San Luis Valley, Colorado, from spaceborne InSAR observations. Water Resour Res 52(5):3623–3636

Conway BD (2016) Land subsidence and earth fissures in south-central and southern Arizona, USA. Hydrogeol J 24(3):649–655

Dehghani M, Valadan Zoej MJ, Entezam I, Mansourian A, Saatchi S (2009) InSAR monitoring of progressive land subsidence in Neyshabour, Northeast Iran. Geophys J Int 178(1):47–56

DuRoss CB, Kirby SM (2004) Reconnaissance investigation of ground cracks along the Western margin of Parowan Valley, Iron County, Utah. Utah Geological Survey, Salt Lake City, UT

Faunt CC, Belitz K, Hanson RT (2009) Development of a three-dimensional model of sedimentary texture in valley-fill deposits of Central Valley, California, USA. Hydrogeol J 18(3):625–649. https://doi.org/10.1007/s10040-009-0539-7

Faunt CC, Sneed M, Traum J, Brandt JT (2016) Water availability and land subsidence in the Central Valley, California, USA. Hydrogeol J 24(3):675–684

Fetter CW (2018) Applied hydrogeology. Waveland, Long Grove, IL,

Forster RR (2006) Land subsidence in Southwest Utah from 1993 to 1996 measured with interferometric synthetic aperture radar (InSAR), vol 6, no. 5. Utah Geological Survey, Salt Lake City, UT

Helm DC (1975) One-dimensional simulation of aquifer system compaction near Pixley, California: 1. constant parameters. Water Resour Res 11(3):465–478

Holzer TL, Galloway DL (2005) Impacts of land subsidence caused by withdrawal of underground fluids in the United States. Humans Geol Agents 16:87–99

Intrieri E, Gigli G, Nocentini M, Lombardi L, Mugnai F, Fidolini F, Casagli N (2015) Sinkhole monitoring and early warning: an experimental and successful GB-InSAR application. Geomorphology 241:304–314. https://doi.org/10.1016/j.geomorph.2015.04.018

Jacob CE (1940) On the flow of water in an elastic artesian aquifer. Trans Am Geophys Union 21(2):574. https://doi.org/10.1029/tr021i002p00574

Khan AS, Khan SD, Kakar DM (2013) Land subsidence and declining water resources in Quetta Valley, Pakistan. Environ Earth Sci 70(6):2719–2727

Kiseleva E, Mikhailov V, Smolyaninova E, Dmitriev P, Golubev V, Timoshkina E, Hooper A, Samiei-Esfahany S, Hanssen R (2014) PS-InSAR monitoring of landslide activity in the Black Sea coast of the Caucasus. Procedia Technol 16:404–413. https://doi.org/10.1016/j.protcy.2014.10.106

Knudsen T, Inkenbrandt P, Lund W, Lowe M, Bowman S (2014) Investigation of landsubsidence and earth fissures in Cedar Valley, Iron County, Utah, vol 150. Utah Geological Survey, Salt Lake City, UT

Lanari R, Casu F, Manzo M, Zeni G, Berardino P, Manunta M, Pepe A (2007) An overview of the small BAseline subset algorithm: a DInSAR technique for surface deformation analysis. Pageoph Topical Volumes, pp 637–661. https://doi.org/10.1007/978-3-7643-8417-3_2

Marston TM (2017) Water resources of Parowan Valley Iron County, Utah. US Geol Surv Sci Invest Rep 2017-5033

Massonnet D, Feigl KL (1998) Radar interferometry and its application to changes in the Earth's surface. Rev Geophys 36(4):441–500

Ortiz-Zamora D, Ortega-Guerrero A (2010) Evolution of long-term land subsidence near Mexico City: review, field investigations, and predictive simulations. Water Resour Res 46(1)

Oviatt CG (1997) Lake Bonneville fluctuations and global climate change. Geology 25(2):155–158

Poland JF, Lofgren BE, Ireland RL, Pugh RG (1975) Land subsidence in the San Joaquin Valley, California, as of 1972. US GeolSurv Prof Pap 437-H, 77 pp

Powell AK (ed) (1994) Utah history encyclopedia. University of Utah Press, Salt Lake City, UT

Riley FS (1969) Analysis of borehole extensometer data from Central California. Int Assoc Sci Hydrol Publ 89:423–431

Riley FS (1998) Mechanics of aquifer systems—The scientific legacy of Joseph F. Poland. In Land subsidence case studies and current

research: Proceedings of the Dr. Joseph F. Poland Symposium on Land Subsidence, Association of Engineering Geologists Special Publ., vol 8, Star Publ., Belmont, CA, pp 13–27

Rogers DH, Aguilar J, Kisekka I, Barnes PL, Lamm FR (2015) Agricultural crop water use. In: Proceedings of the 27th annual Central Plains Irrigation Conference, CPIA, Colby, KS, pp 17–18

Ryder I, Parsons B, Wright TJ, Funning GJ (2007) Post-seismic motion following the 1997 Manyi (Tibet) earthquake: InSAR observations and modelling. Geophys J Int 169(3):1009–1027. https://doi.org/10.1111/j.1365-246x.2006.03312.x

Sandwell D, Mellors R, Tong X, Wei M, Wessel P (2011) Open radar interferometry software for mapping surface deformation. Eos 92(28):234–235

Shah AK, Boyd OS (2018) Depth to basement and thickness of unconsolidated sediments for the western United States: initial estimates for layers of the U.S. Geological Survey National Crustal Model. US Geol Surv Open File Rep 2018–1115

Shirzaei M, Ellsworth WL, Tiampo KF, González PJ, Manga M (2016) Surface uplift and time-dependent seismic hazard due to fluid injection in eastern Texas. Science 353(6306):1416–1419

Simons M (2002) Coseismic deformation from the 1999 mw 7.1 Hector Mine, California, earthquake as inferred from InSAR and GPS observations. Bull Seismol Soc Am 92(4):1390–1402. https://doi.org/10.1785/0120000933

Smith R, Li J (2021) Modeling elastic and inelastic pumping-induced deformation with incomplete water level records in Parowan Valley, Utah. J Hydrol 601:126654

Smith RG, Knight R, Chen J, Reeves JA, Zebker HA, Farr T, Liu Z (2017) Estimating the permanent loss of groundwater storage in the southern San Joaquin Valley, California. Water Resour Res 53(3):2133–2148

Sneed M (2001) Hydraulic and mechanical properties affecting groundwater flow and aquifer-system compaction, San Joaquin Valley, California, vol 1. US Geological Survey, Reston, VA

Scott, R. F. (1963). Principles of Soil Mechanics, Addison-Wesley. Reading, Massachusetts, 54.

Teatini P, Tosi L, Strozzi T, Carbognin L, Cecconi G, Rosselli R, Libardo S (2012) Resolving land subsidence within the Venice lagoon by persistent scatterer SAR interferometry. Phys Cheme Earth, Parts A/B/C 40:72–79

Terzaghi, K. A. R. L. (1925). Principles of soil mechanics. Engineering News-Record, 95(19-27):19–32.

Van Niekerk HJ, Van der Walt IJ (2006) Dewatering of the far west Rand dolomitic area by gold mining activities and subsequent ground instability. Land Degrad Dev 17(4):441–452

Yin Y, Zheng W, Liu Y, Zhang J, Li X (2010) Integration of GPS with InSAR to monitoring of the Jiaju landslide in Sichuan, China. Landslides 7(3):359–365. https://doi.org/10.1007/s10346-010-0225-9

Yin J, Yu D, Wilby R (2016) Modelling the impact of land subsidence on urban pluvial flooding: a case study of downtown Shanghai, China. Sci Total Environ 544:744–753

Youssef et al (2013) Earth fissures in Wadi Najran, Kingdom of Saudi Arabia. Nat Hazards 71(3). https://doi.org/10.1007/s11069-013-0991-5